Extended data figure

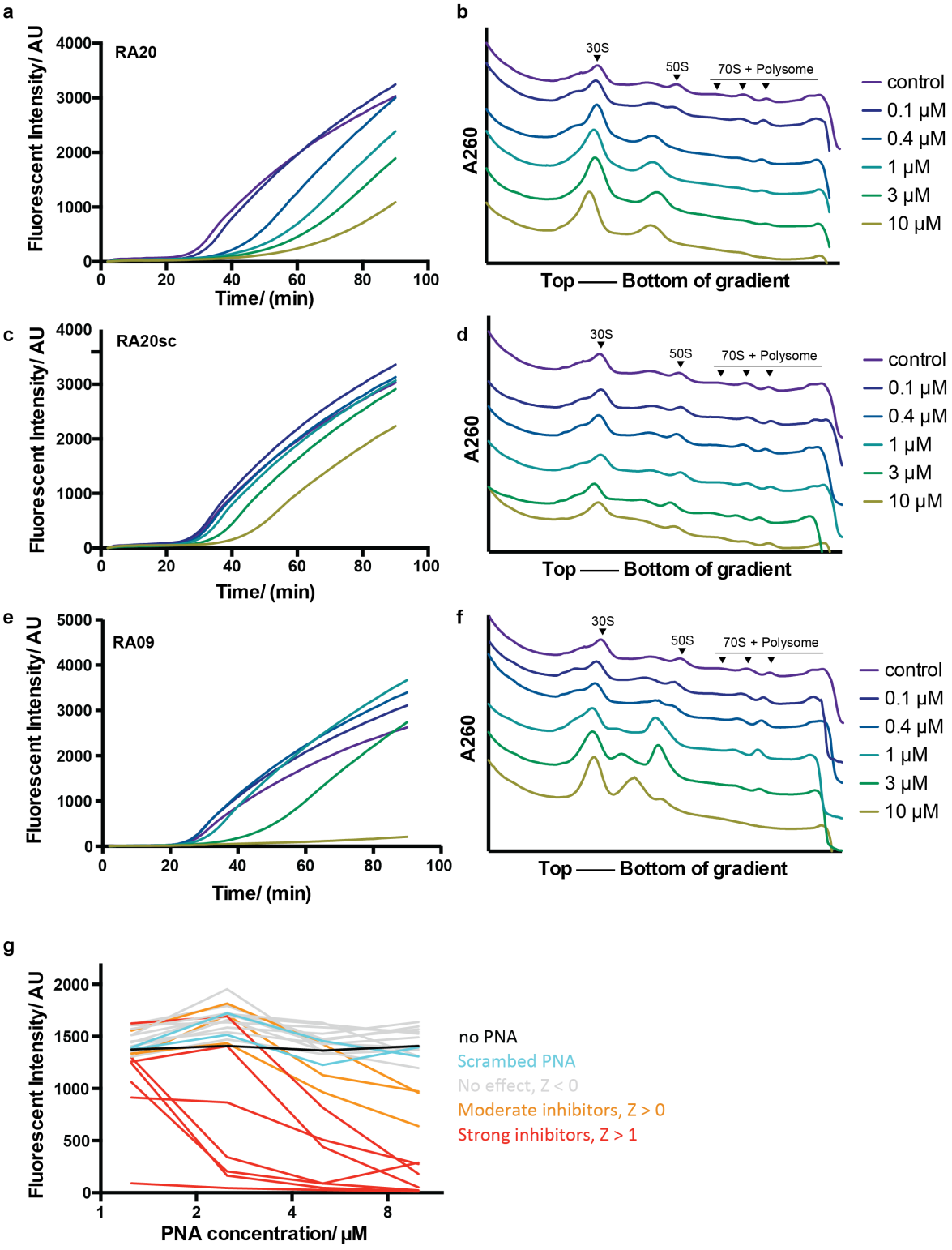

Extended Data Fig.1 | Titration of PNA in iSAT assay

Extended Data Fig.1 (continued) Fluorescent traces for iSAT reaction with RA20 (**a**), scrambled RA20 (RA20sc) (**c**) and RA09 (**e**) and corresponding sucrose gradient profiles (**b d f**). The PNAs were titrated from 10 μM to 0.1 μM with three-fold dilution. The 30S, 50S, 70S and polysome peaks were marked on the gradient profile for the control sample. The traces in **a-f** are colored by the concentration of the PNA according to the rightmost color legends. **g**) End-point fluorescence for PNA library at 10, 5, 2.5 and 1.25 μM. The curves are colored according to the *Z*-scores in **Fig.1 h**.

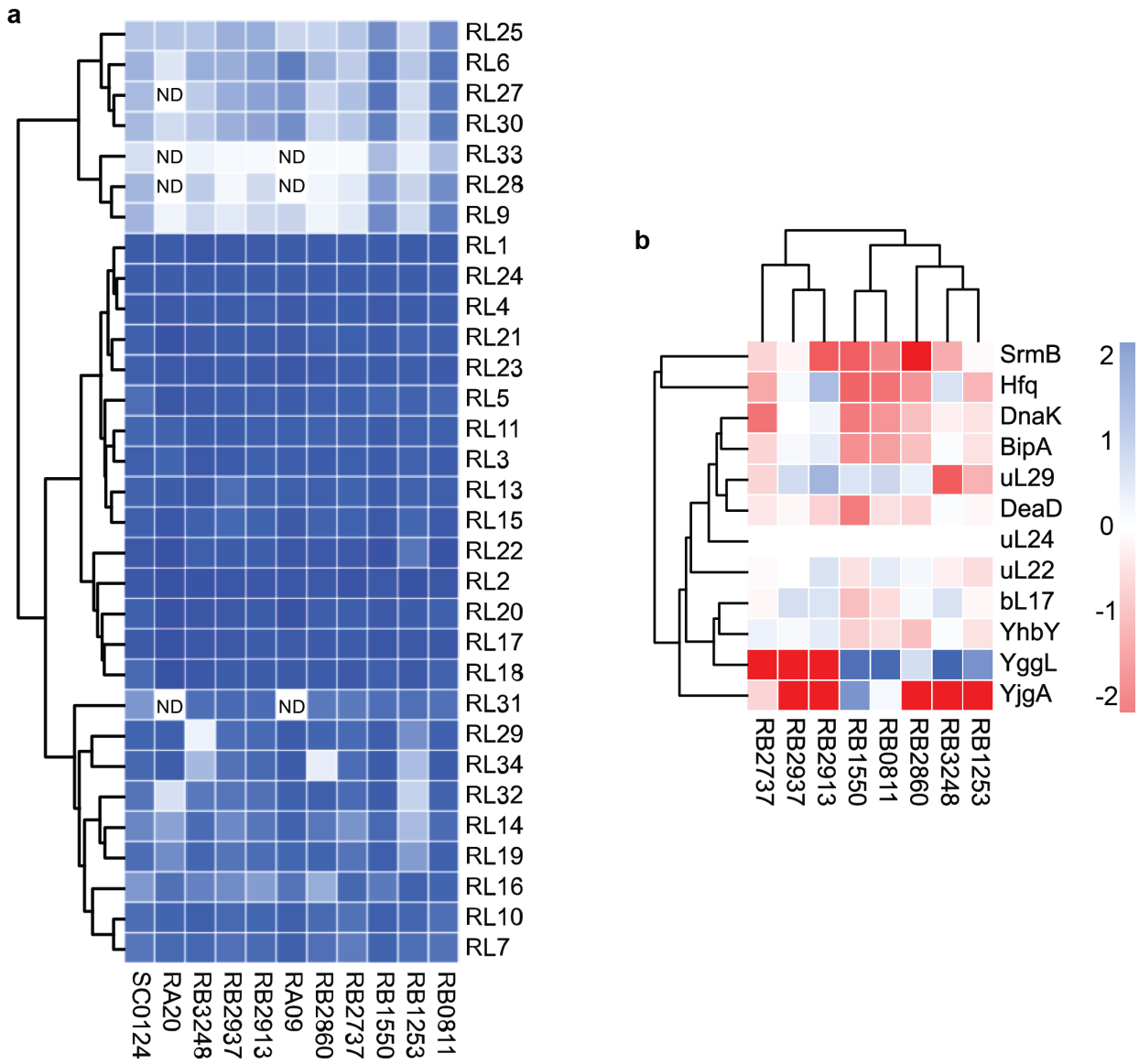

Extended Data Fig.2 | Proteomics analysis of intermediate fractions

Extended Data Fig.2 (continued) a) Heatmap representation for quantitative proteomics analysis for r-proteins. The abundance was normalized to N15 samples then uL24 abundance in each sample. (Blue:1, white: 0). ND means there is no peptide detected in either N14 or N15 peptide search. **b**) Peptide spectrum matches (PSMs) for selected assembly factors. The PSMs were normalized to total N14 PSMs then control sample. The color scheme from red to blue represents the $\log_2$ fold change ($\log_2$FC).

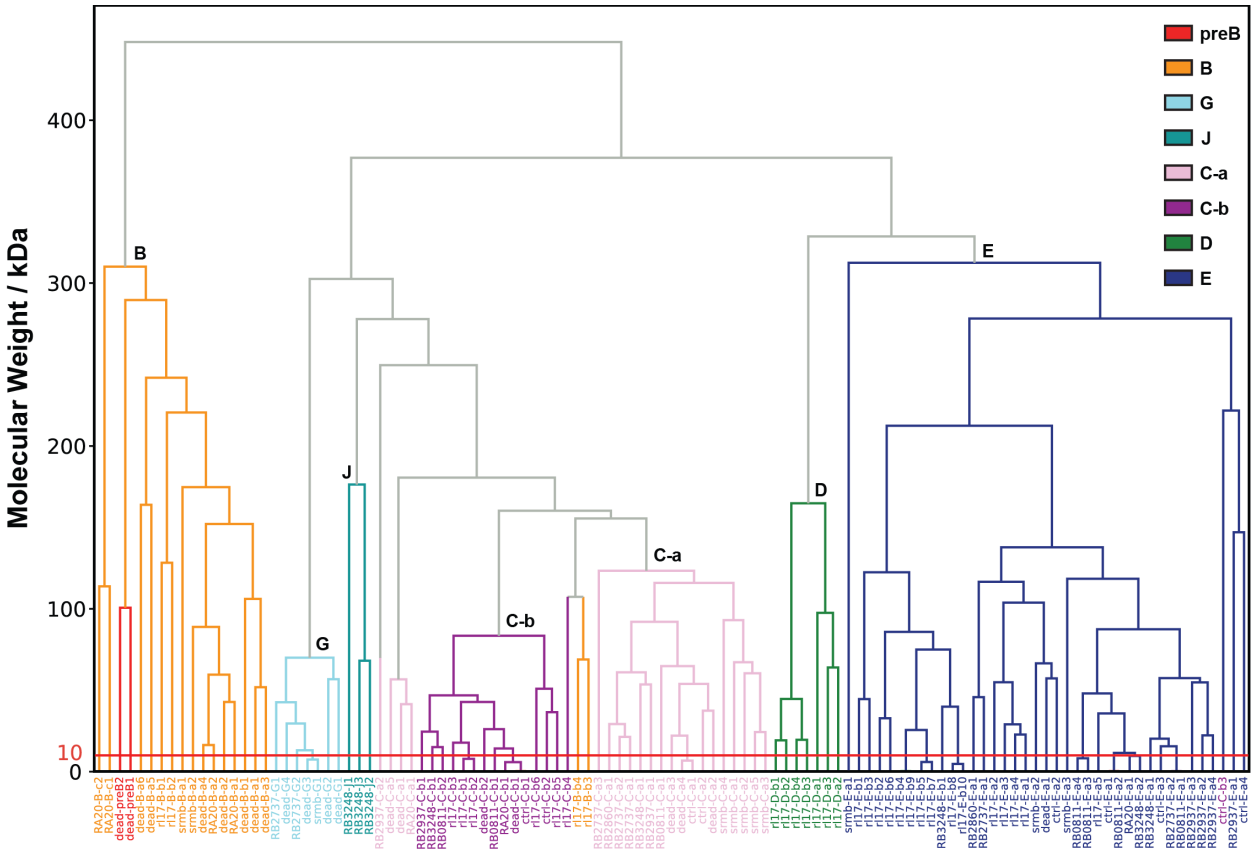

Extended Data Fig.3 | Comparison with previous classes

The Euclidean distance matrix, based on molecular weight in kDa, was calculated among 47 density maps and previous density maps from bL17-depletion, Δ*deaD* and Δ*srmB* datasets. The dendrogram resulting from hierarchical clustering is displayed, with the 8 main class branches colored accordingly.

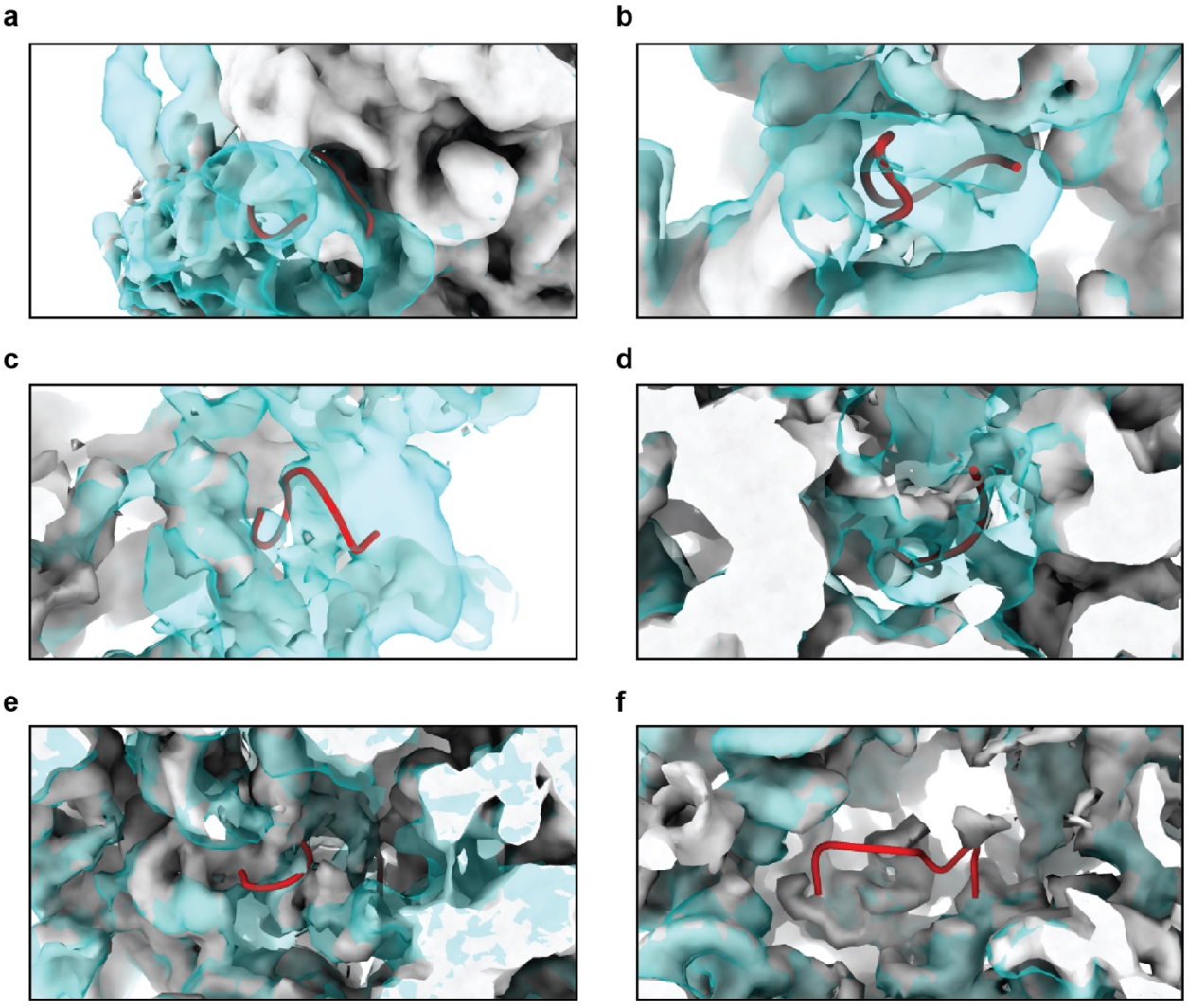

Extended Data Fig.4 | PNA targeting sites in control average map

a-g) shows the PNA targeting site (red ribbons) on corresponding average map (from **a** to **g**: RA20, RB3248, RB2937, RB2860, RB2737 and RB0811, shown in light grey density). The control average map was shown in transparent cyan density.

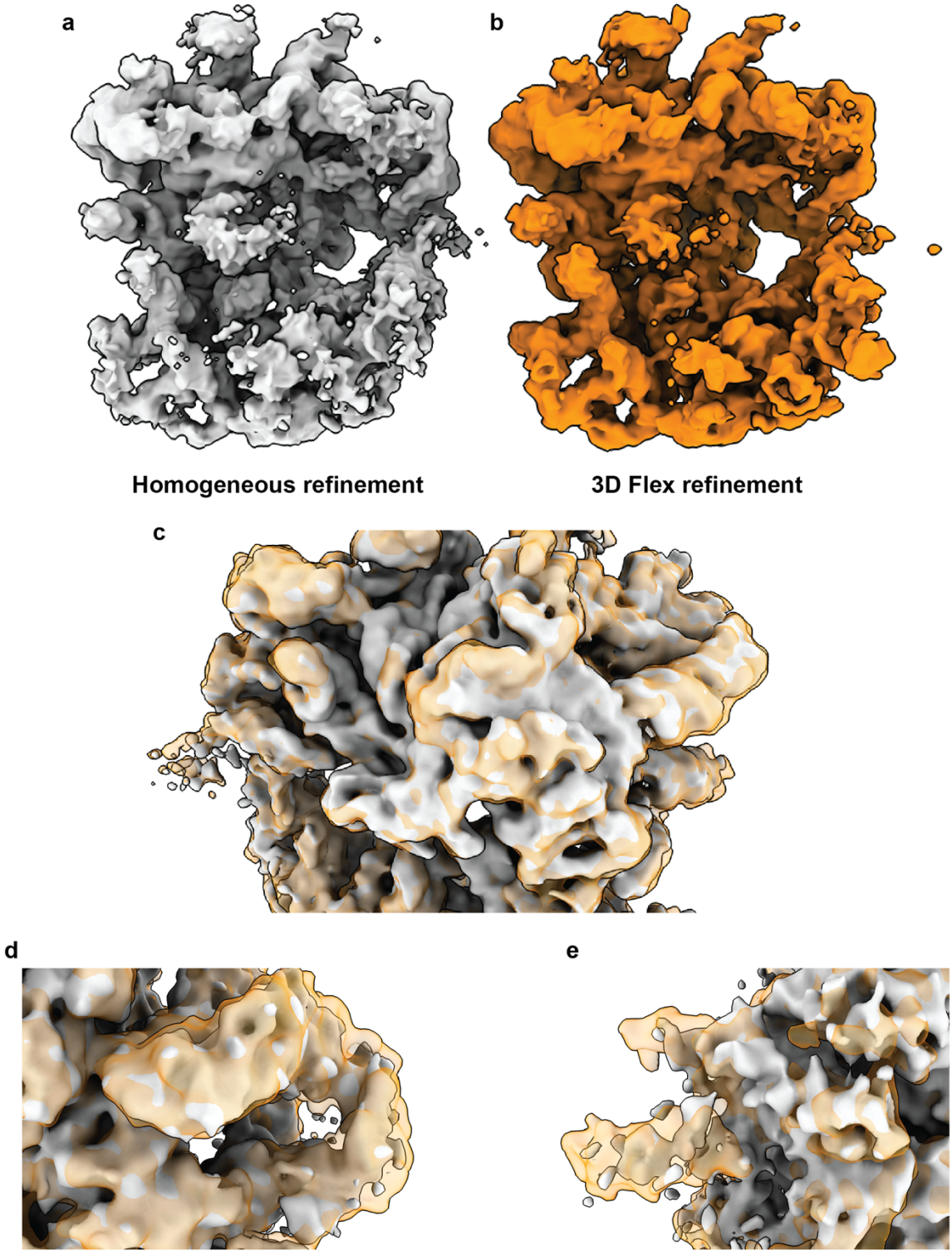

Extended Data Fig.5 | Comparison between density map from homogeneous refinement and from 3D Flex refinement for RA20-B-c class

Extended Data Fig.5 (continued) The homogeneous refinement and 3D flex refinement map for RA20-B-c class are shown in **a**) and **b**) respectively. Zoomed in comparison for **c**) domain I/II, **d**) domain III, and **e**) domain VI are shown with map from 3D flex refinement in orange transparent volume and map from homogeneous refinement in light grey.

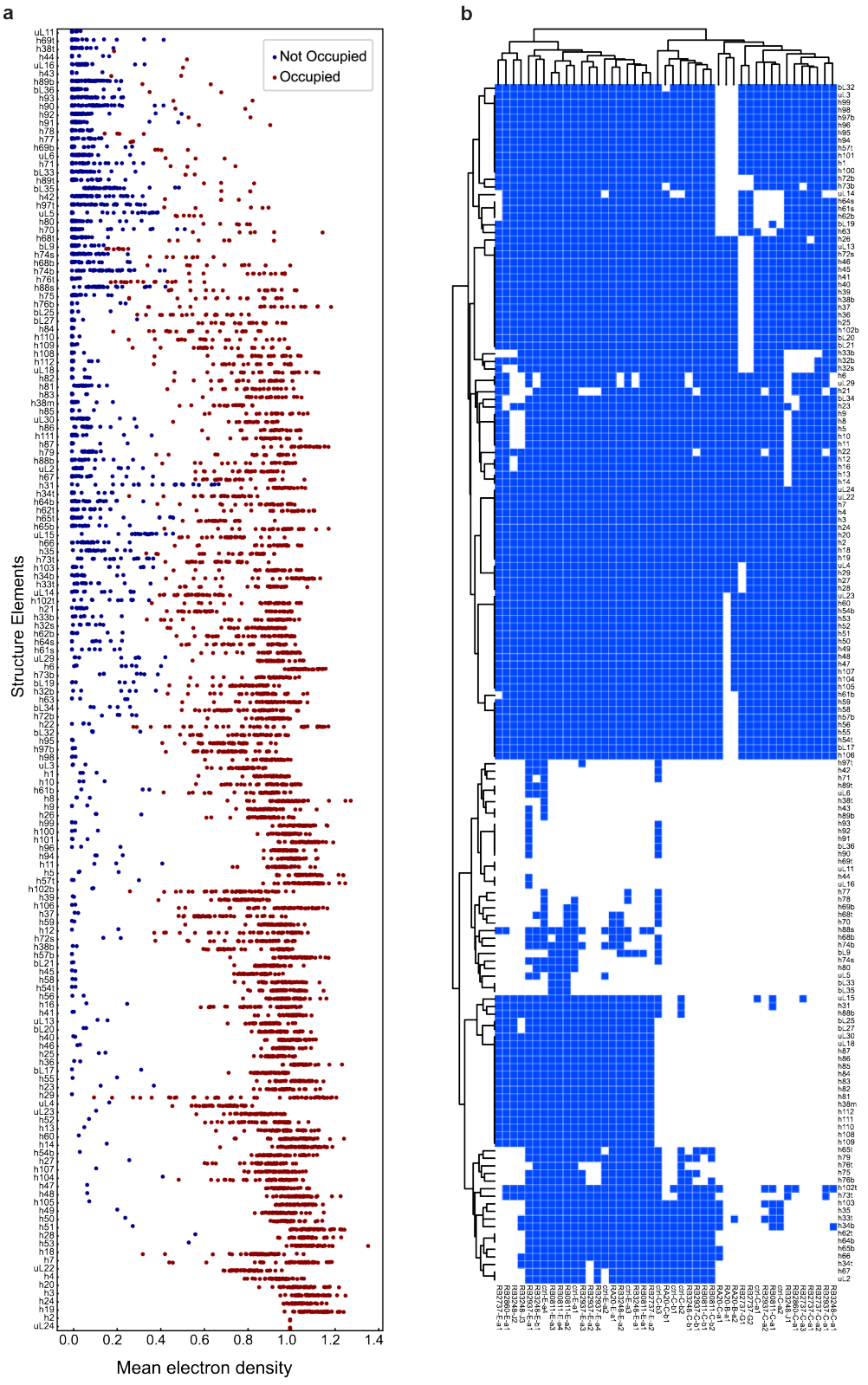

Extended Data Fig.6 | Generation of Binarized Occupancy Matrix

Extended Data Fig.6 (continued) a) Strip plot for each structure elements. There are 157 structure elements on the y-axis. Each dot in one strip represents the occupancy (x-axis) for one structure element in one electron density map. The non-occupied dots were colored blue, while the occupied dots were colored red. b) Occupancy of 45 intermediate density maps (without RA20-B-c classes) from PNA-inhibited dataset in terms of the 157 structure elements, binarized with threshold in **a**) and used for dependency analysis.

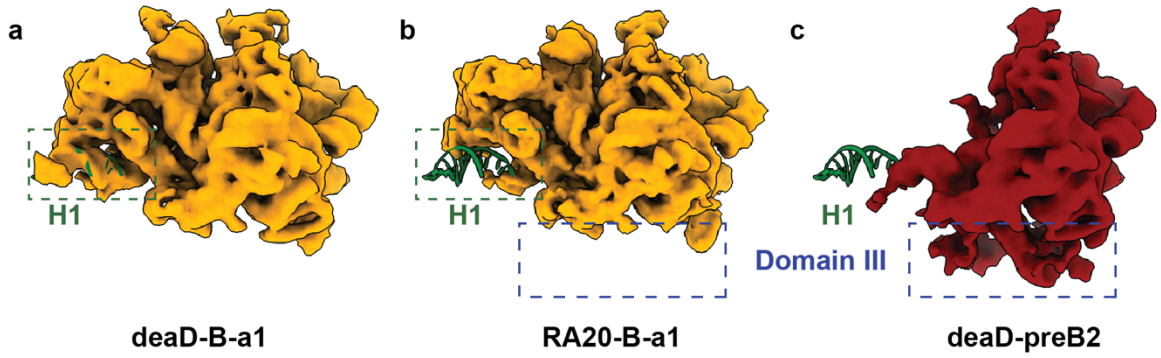

Extended Data Fig.7 | Missing of H1 density in different classes

Back view of **a**) deaD-B-a1, **b**) RA20-B-a1 and **c**) deaD-preB2 with atomic model of H1 helix (green), highlighted in green boxes. The empty and partial domain III density in b) and c) were highlighted in blue boxes.

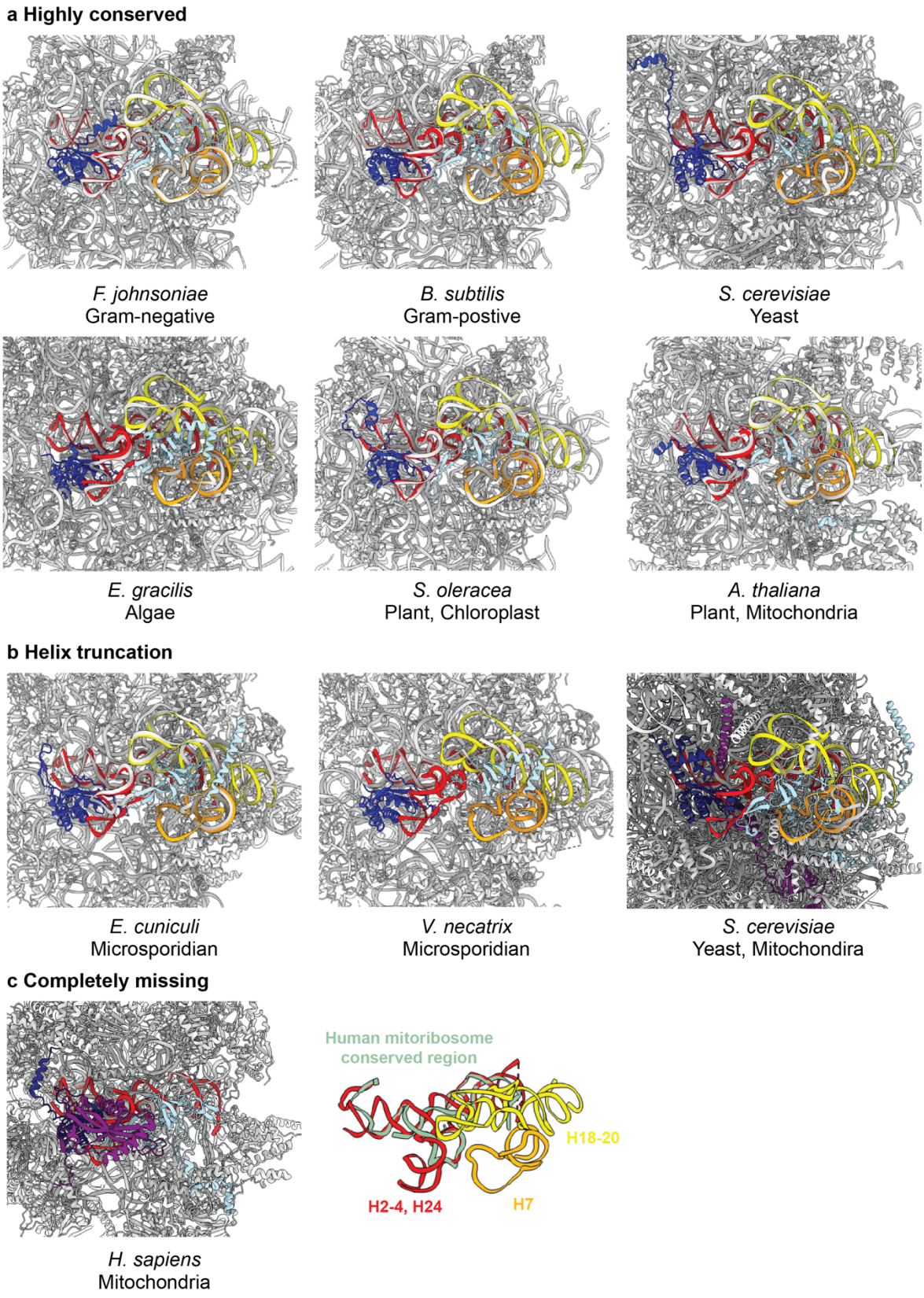

Extended Data Fig.8 | Smallest consensus core in different species

Extended Data Fig.8 (continued) The LSU models for different species are shown and classified according to the similarities in helix structure, **a**) highly conserved, **b**) truncated and **c**) completely missing. The rRNA helices in *E. coli* smallest consensus core identified in this work is shown in colorful ribbons (red: H2-4, H24, orange: H7, yellow: H18-20). The LSU rRNA in other species are shown in light grey. The uL22 and uL24 homologs for *E. coli* in other species are shown in dark blue and light blue respectively. The uL23 in yeast mitoribosome and mL45 in human mitoribosome were colored purple for easy visualization. The PDB IDs are (in sequential order): 7JIL, 6HA1, 5JCS, 6ZJ3, 5X8P, 6XYW, 7QEP, 6RM3, 5MRC, 7QI4. For human mitoribosome, the rRNA homologous regions are colored green in the right panel and overlaid with H2-4, H24, H7 and H18-20 in *E. coli*. The secondary structures were drawn using RiboVision2.

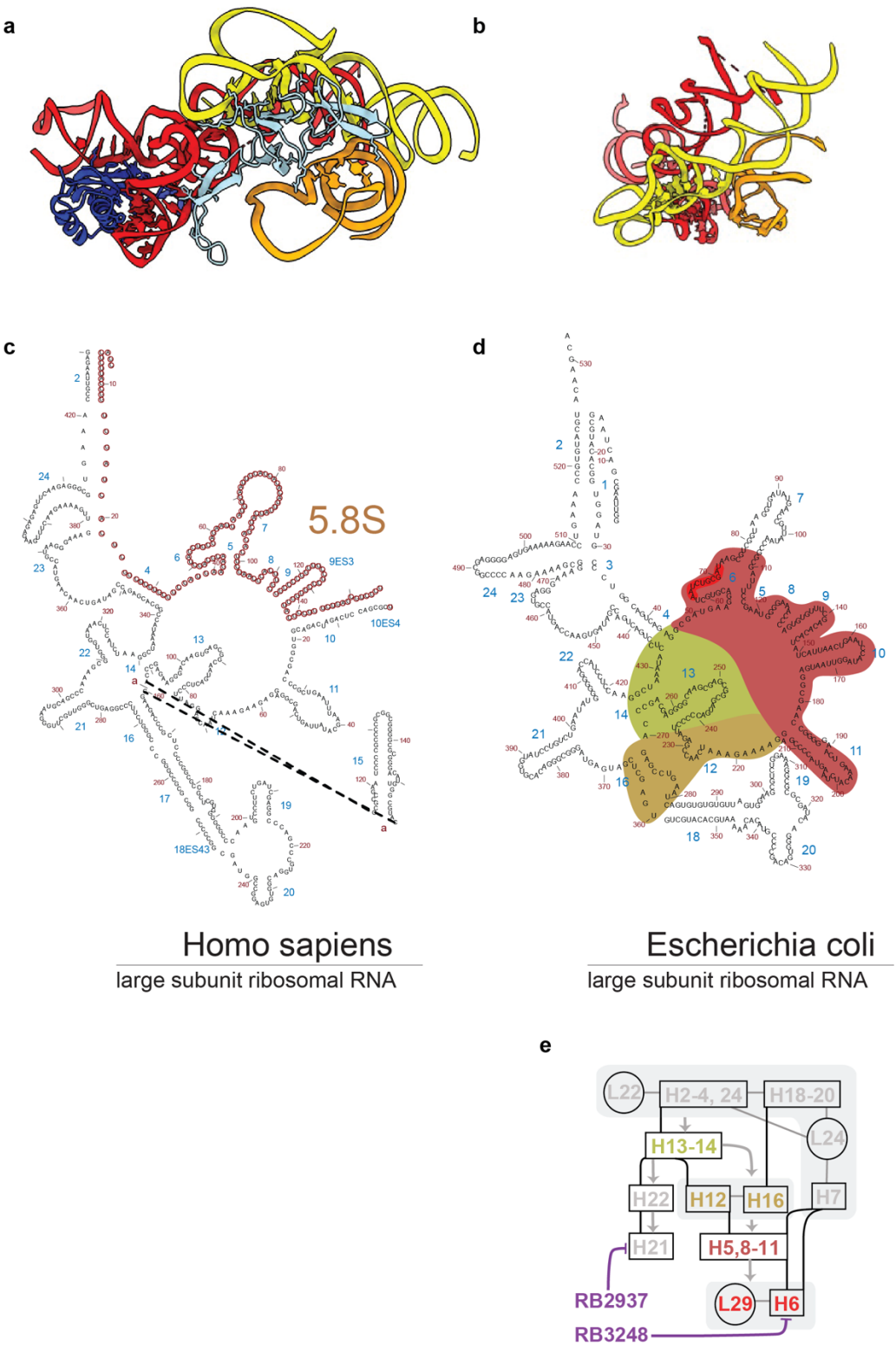

Extended Data Fig. 9 | Smallest consensus core and 5.8S

Extended Data Fig. 9 (continued)

a) Back and **b**) side views of the smallest consensus core. Secondary structure for part of domain I rRNA in **c**) *H. sapiens* and **d**) *E. coli*. The 5.8S in *H. sapiens* is colored brown. The helix defect in *E. coli* LSU with RB3248 are marked with according to dependency in **e**).

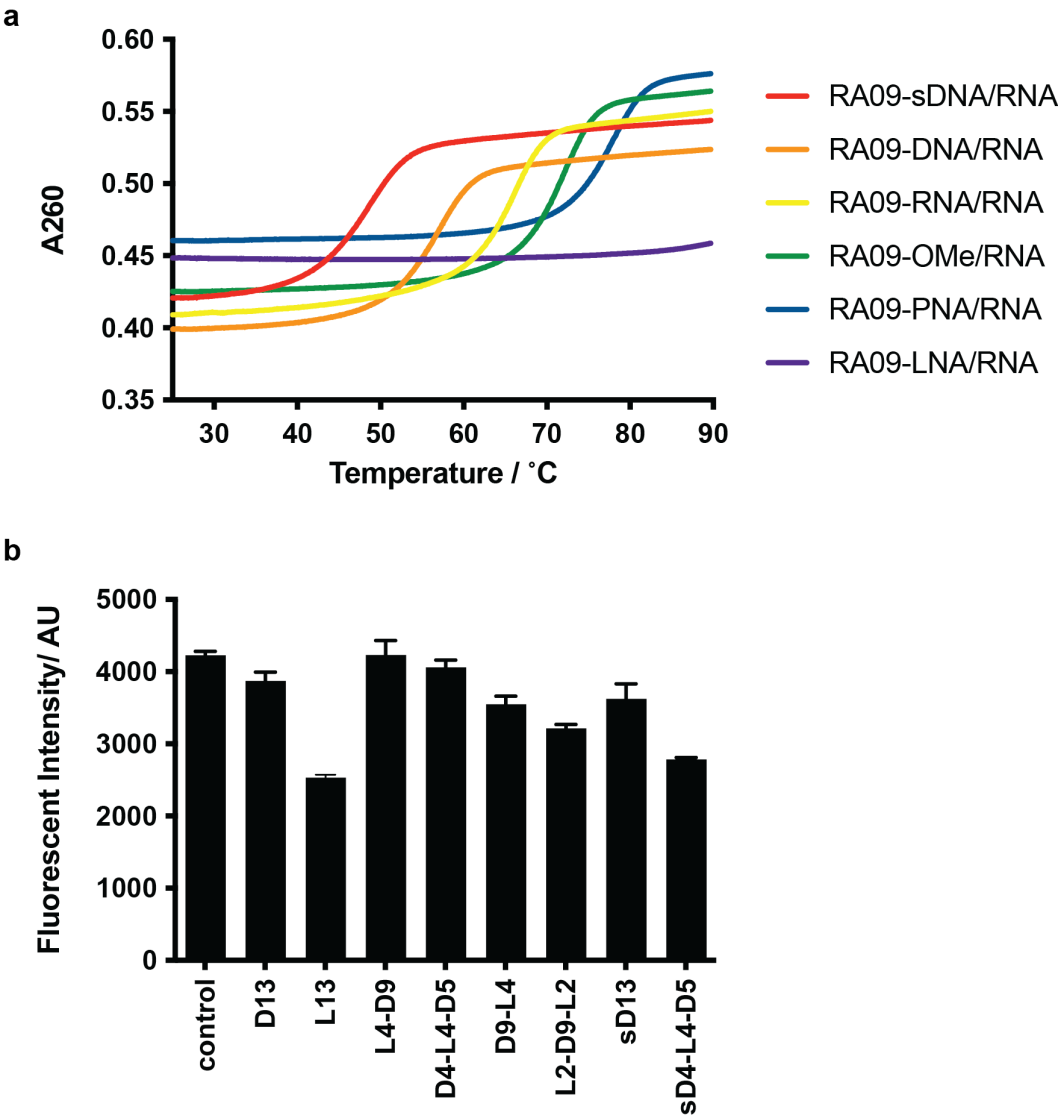

Extended Data Fig. 10 | Properties of ASO analogs

a) Melting curves of ASO analogs of RA09 to the RNA target were measured at 3 μM in iSAT buffer. The temperature ranges from 25 to 85 ˚C and during the temperature ramping, the A260 nm was measured. **b**) End-point fluorescence of RA20 with different locked site and phosphorothioate (PS) backbones. L*m*D*n* means the locked state starting from 5' end of the ASO. For example, L4D9, means first four ribose for RNA20 are 2'-5' locked, while the rest of it remained DNA backbone. "s" denotes the backbone of the ASO is replaced with PS.

Supplementary table

Supplementary Table.1a Sequences for 1st library

Name	Sequence	Length	GC
RA01	GTTTGACGCTCAAAGAATT	19	0.37
RA03	CCTCTACGAGACTCAA	16	0.50
RA04	GGAGGTGATCCAACC	15	0.60
RA05	CACTACAAAGTACGCTTCT	19	0.42
RA06	ATTGCTTATCACGCGT	16	0.44
RA07	CAAACCAGCAAGTGGCGTCC	20	0.60
RA08	CTTAACCTCACAACCCGA	18	0.50
RA09	GGAGTATTTAGCCTTG	16	0.44
RA10	CGAAACAGTGCTCTAC	16	0.50
RA11	GAACAGCCATACCCTT	16	0.50
RA12	GTAAGGTTAAGCCTCA	16	0.44
RA13	GCTACTGCCGCCAGGC	16	0.75
RA14	TCTAGACGAAGGGGAC	16	0.56
RA15	TTATCGTTACTTATG	15	0.27
RA16	GCGAGTTCAATTTC	14	0.43
RA18	TTCCATTCAGAACC	14	0.43
RA19	CGACATCGAG	10	0.60
RA20	TAGTCGCTTAACC	13	0.46
RA21	GTTACTCTTTA	11	0.27
RA22	ACAACCGTCG	10	0.60
RA23	CAGGAACCCTT	11	0.55
RA24	TTTCCCACTTAA	12	0.33
RA25	GGTTTGGGGTA	11	0.55
RA26	TTATAGTTACGGC	13	0.38

Supplementary Table.1b Sequences for 2nd library

Name	Sequence	Length	GC
SC0124	CGACATAGTCCAC	13	0.54
SC0180	GAGATCGATGCCC	13	0.62
RB2263	ACATCCTGGCTGT	13	0.54
RB2206	GCCGACTCGACCA	13	0.69
RB2172	TGCATGGTTTAGC	13	0.46
RB1550	TTGCAGCCAGCTG	13	0.62
RB3248	CTTATCGCAGATT	13	0.38
RB3202	CATTCGGAAATCG	13	0.46
RB3152	AACCTATGGATTC	13	0.38
RB3000	GTATCGCGCGCCT	13	0.69
RB2937	CGTGTCCCGCCCT	13	0.77
RB2913	CCCCCATATTCAG	13	0.54
RB2860	CGGTACTGGTTCA	13	0.54
RB2789	ACTGCTTGTACGT	13	0.46
RB2744	CCCATTATACAAA	13	0.31
RB2737	TCGCTGACCCATT	13	0.54
RB1461	CCCATCAATTAAC	13	0.38
RB1401	CCGTTATAGTTAC	13	0.38
RB1253	TCACGGGGTCTTT	13	0.54
RB1200	CACCTATCCTACA	13	0.46
RB0811	GAGCCGACATCGA	13	0.62
RA09-PNA	GGAGTATTTAGCCTTG	16	0.44
RA20-PNA	TAGTCGCTTAACC	13	0.46
RA20sc-PNA	ATTGGCTCATCAC	13	0.46

Supplementary Table.2 Metadata for electron density maps

Name	*particle number*	*resolution/ Å*	*EMD*
ctrl-C-a1	2120	5.8	EMD-44483
ctrl-C-a2	1910	6.2	EMD-44485
ctrl-C-b1	5675	4.7	EMD-44487
ctrl-C-b2	3672	4.8	EMD-44488
ctrl-C-b3	1633	6.0	EMD-44564
ctrl-E-a1	5153	4.3	EMD-44565
ctrl-E-a3	1732	5.1	EMD-44566
ctrl-E-a2	1631	6.1	EMD-44567
ctrl-E-a4	1006	6.3	EMD-44568
RA20-B-a1	3022	4.2	EMD-44569
RA20-B-a2	4218	3.9	EMD-44570
RA20-B-c1	3904	5.2	EMD-44571
RA20-B-c2	3608	6.1	EMD-44572
RA20-C-a1	2201	4.4	EMD-44573
RA20-C-b1	2754	4.6	EMD-44574
RA20-E-a1	1898	4.2	EMD-44575
RB0811-C-a1	1707	6.1	EMD-44576
RB0811-C-b1	1457	5.9	EMD-44578
RB0811-C-b2	1430	6.1	EMD-44579
RB0811-E-a1	7066	4.6	EMD-44580
RB0811-E-a2	3430	4.7	EMD-44584
RB0811-E-a3	1857	5.1	EMD-44581
RB0811-E-a4	1236	5.5	EMD-44582
RB2737-C-a1	2743	4.4	EMD-44583
RB2737-C-a2	2558	4.7	EMD-44604
RB2737-C-a3	1979	5.3	EMD-44605

RB2737-E-a1	6682	4.2	EMD-44606
RB2737-E-a2	2195	4.8	EMD-44607
RB2737-G1	2437	4.7	EMD-44608
RB2737-G2	2468	4.9	EMD-44609
RB2860-C-a1	13429	4.3	EMD-44610
RB2860-E-a1	3174	5.5	EMD-44611
RB2937-C-a1	1661	6.9	EMD-44612
RB2937-C-a2	1418	7.5	EMD-44613
RB2937-C-b1	5244	5.1	EMD-44614
RB2937-E-a1	2568	5.9	EMD-44615
RB2937-E-a2	2507	6.2	EMD-44616
RB2937-E-a3	1451	6.3	EMD-44617
RB2937-E-a4	7355	5.0	EMD-44618
RB3248-C-a1	1811	6.5	EMD-44619
RB3248-C-b1	1942	5.1	EMD-44620
RB3248-E-a1	2362	4.9	EMD-44621
RB3248-E-a2	1983	5.0	EMD-44622
RB3248-E-b1	1796	4.9	EMD-44623
RB3248-J1	5827	4.2	EMD-44624
RB3248-J2	2415	5.6	EMD-44625
RB3248-J3	2461	5.3	EMD-44626